DOI: 10.13009/EUCASS2017-609

7TH EUROPEAN CONFERENCE FOR AERONAUTICS AND AEROSPACE SCIENCES (EUCASS)

DOI: ADD DOINUMBER HERE

Analysis of coaxial-flame response during transverse combustion instability

Annafederica Urbano⋆ *and Quentin Douasbin*⋆ *and Laurent Selle*⋆†
⋆*Institut de Mécanique des Fluides de Toulouse (IMFT), Université de Toulouse, CNRS, INPT, UPS, Toulouse, France*
annafederica.urbano@imft.fr · quentin.douasbin@imft.fr · laurent.selle@imft.fr
†Corresponding author

Abstract

This paper presents the investigation of flame response during a transverse combustion instability in a small-scale rocket engine via numerical simulation. The computation is performed in the framework of Large-Eddy Simulation with the objective to understand the physical mechanisms driving the contribution of the unsteady combustion to the unstable mode. Two simulations are considered: first, a computation of the full engine, including the injection manyfold, the 42 coaxial injectors, the combustion chamber and the outlet nozzle. Then a single injector is considered for the scrutiny of individual flame response. The analysis of the unstable transverse mode in the full configuration reveals the contribution of individual flames through a budget of acoustic energy. The single-injector configuration exhibits the different roles of the hydrogen and oxygen flows in the flame response.

1. Introduction

Avoiding the occurrence of combustion instabilities (CI) is one of the most critical requirements in the development of high-performance combustion engines. Because only a minute fraction (as little as 10^{-4}) of the energy released by combustion is enough to provoke a destructive instability,[1] any engine will most likely be unstable –and dangerously close to failure– within a certain range of operating conditions. For example, the development of the F1 engine that brought man to the Moon during the Apollo program, required 1332 full-scale hot-fire tests and 108 injector design changes before meeting both stability and performance requirements.[2,3]

Combustion instabilities result from the constructive coupling between acoustic waves and unsteady heat release rate. There are essentially two conditions for CI to occur, namely

1. The first one attributed to Rayleigh,[4] states that the integral over a period of the oscillation of the product of pressure (p') and heat release rate (q') fluctuations must be positive. This imposes a constraint on the phase (or the time delay) between p' and q'.

2. The second condition is that the energy fed into acoustics by combustion must overcome the fluxes at the boundaries and the various internal losses.[5] Thus, the gain of the destabilising process must exceed a certain threshold value.[6]

These criteria can be expressed in an accurate mathematical form by studying the conservation equation for disturbance energy, (cf. Section 3). Unfortunately, it is almost impossible to determine the stability map and stability margins of an engine at the design stage with current tools. Guidelines for design and flight certification in the aerospace industry are still based on experimental knowledge[7] dating back to the 1940's and 60's. CI are usually classified according to the frequency of the oscillations. For instabilities below 100 Hz, the term chugging is common, while above several hundreds or thousands of cycles per second, names such as screaming or screeching are often used. While the low-frequency CI are relatively easy to avoid, high-frequency CI are much harder to mitigate, especially those with a structure transverse to the mean flow. It is therefore critical to understand what drives transverse modes. Sometimes, these transverse modes cannot be avoided even with proper design so that they must be damped by the addition of cavities[8] or baffles[3,9] in the combustion chamber. There have been many attempts to predict transverse modes with low-order models, but lack of knowledge about the flame response limits these studies to parametric variations for n and τ.[10–12] Understanding how flames respond to transverse excitation is a crucial research imperative. Indeed, for transverse modes, both pressure, axial and tangential velocity fluctuations may affect the flame, which would mean that

DOI: 10.13009/EUCASS2017-609

three input variables may be necessary to model the flame response rather than only one as in the standard model of Crocco.

Some insight was gained by the experimental investigation of multiple-injector combustion chambers with optical access[13–15] but as these configurations have only a few injectors, it is often necessary to force acoustics externally because transverse CI do not occur naturally. With regard to numerical simulations, there have been some attempts to compute flame responses[16,17] but, as explained by,[11] no LES of a full engine has been published to date. This frontier has now been breached by[18] who performed the first LES of a full rocket engine from the propellant injection domes, through the injectors and all the way to the exit nozzle.

The objective of the present work is to use this LES database to study high-frequency transverse CI. The configuration is first presented in Section 2 together with the operating conditions and the database of numerical simulations. Then, in Section 3, the driving and damping terms of the acoustic disturbance equation are analysed. Finally, preliminary results on the forced response of a single coaxial injector are given in Section 4.

2. Configuration and numerical setup

The present work uses the LES database of Urbano et al.,[18] which simulates the whole BKD engine, from the injection manifolds to the outlet of the exhaust nozzle. The computational domain is presented in Fig. 1: it includes the 42 coaxial injectors and the whole combustion chamber. The reader is referred to the work of Urbano et al.[18] for details about the numerics, which are only summarised here. The LES is performed with the AVBP-RG code, which solves the

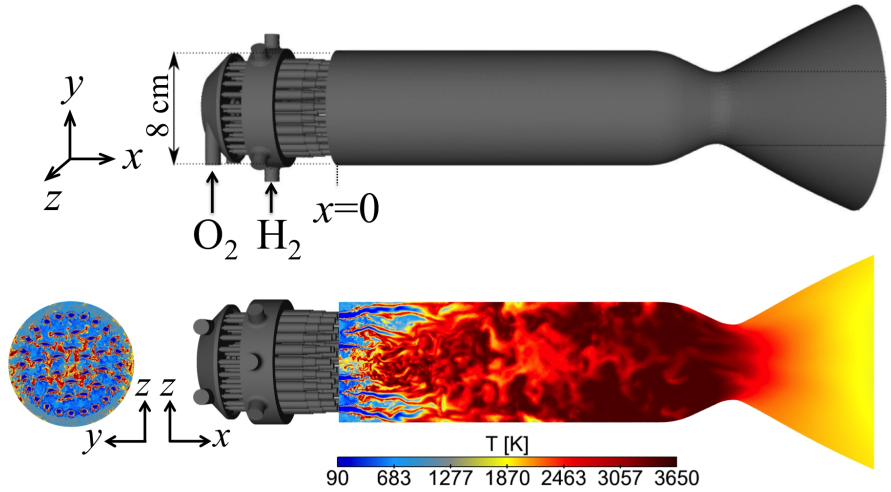

Figure 1: Computational domain for the LES of the whole engine (top). Transverse and longitudinal cut of temperature field (bottom).

compressible Navier-Stokes equations on unstructured meshes. The explicit third-order Taylor-Galerkin scheme called TTG4A[19] is used together with the Wall Adapting Linear Eddy (WALE) model to close the subgrid stress tensor.[20] Given the thermodynamic conditions encountered in liquid rocket engines, a cubic equation of state is necessary. Here we used the Soave-Redlich-Kwong equation[21] together with transport properties relying on the corresponding-state model of Chung et al.[22] Turbulent combustion is modelled in the framework of infinitely-fast chemistry,[23] which is adequate thanks to the very high reactivity of hydrogen and oxygen at high pressure. Finally, this set of equations and models is solved on a 70 M cell mesh.

The operating conditions are summarised in Table 1 where two cases are described: LP1 and LP4. Both have nearly identical propellants' temperatures and differ by their oxidiser to fuel ratio ($r = \dot{m}_{O_2}/\dot{m}_{H_2}$), resulting in different combustion-chamber pressure (p_c). The consequence of this variation in r is that while LP1 is stable, LP4 exhibits a

Table 1: Operating conditions

	Ox./Fuel ratio	$\dot{m}_{H_2}$ [kg.s^{-1}]	T_{H_2} [K]	T_{O_2} [K]	p_c [bar]	Exp. Stability
LP1	4	1.11	94	112	70.3	Stable
LP4	6	0.96	96	111	81.4	Untable

DOI: 10.13009/EUCASS2017-609

strong combustion instability.[24] It was shown by Urbano et al.[18] that this behaviour could be captured by the LES and the instantaneous temperature field shown in Fig. 1 actually corresponds to the unstable LP4 condition. Qualitative features of transverse combustion instabilities are evident, such as the shortening and flattening of the central flames, which are subjected to large transverse velocity fluctuations.

It was observed experimentally and in the LES that the acoustic pressure spectra is dominated by two sharp peaks. It was fairly straightforward to identify the structure of the first peak from the pressure sensors installed in the experiment: it corresponds to the first transverse mode (labeled 1T) of the combustion chamber. Its structure, reconstructed from a Fourier Transform (FT) of the pressure field in the LES is shown in Fig. 2(a). The frequency of

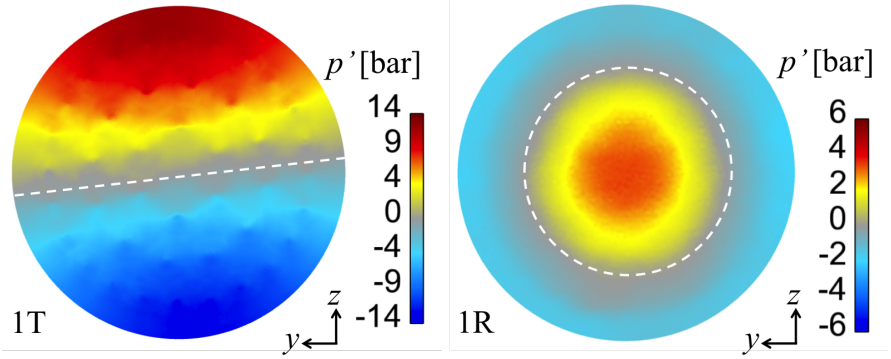

(a) Transverse mode (1T). (b) Radial mode (1R).

Figure 2: Transverse cuts through the chamber showing the spatial structure of the two dominant pressure modes calculated by Fourier Transform during the limit cycle of LP4. Respective frequencies: $f_{1T} = 10\,700$ Hz and $f_{1R} = 21\,400$ Hz. The pressure nodes are marked by the white dashed lines.

this 1T mode in the LES is $f_{1T} = 10\,700$ Hz, which is very close to the experimental value of 10 260 Hz. The second peak in the pressure spectra was exactly at a twice that of the 1T mode. The LES showed that it corresponded to the first radial mode (1R) of the combustion chamber and its structure is presented in Fig 2(b).

For both modes presented in Fig. 2 the location of the pressure nodes is highlighted by a white dashed line. It is important to bear in mind that a flame near these locations will experience large transverse velocity and small pressure fluctuations. Conversely, flames far from the pressure nodal line will be submitted to large pressure and small velocity fluctuations.

3. Analysis of disturbance energy

The objective of this Section is to understand the mechanisms that dictate the stability of the LP1 and LP4 cases. We therefore analyse the simulations of Urbano et al.[18] in the framework of disturbance energy, E_d, which is the extension of the concept of acoustic energy. There are essentially three contributions to the disturbance energy: acoustics, vorticity and entropy (temperature and composition) and an exact transport equation for E_d was initially derived by Myers[25] and later extended by Brear et al.[26] Because we address here transverse and radial modes, entropic perturbations are left out. With the additional assumption of chemical equilibrium, the balance equation for E_d reads:

$$\frac{\partial E_d}{\partial t} + F = R + D. \tag{1}$$

The disturbance energy, E_d, in the control volume V and the flux, F, through its boundary S, write:

$$E_d = \int_V (\rho H' - \overline{\boldsymbol{m}} \cdot \boldsymbol{u}' - p')\, dV \tag{2}$$

$$F = \oint_S \left(\boldsymbol{m}' H' + \overline{\boldsymbol{m} H'}\right) \cdot \boldsymbol{n}\, dS, \tag{3}$$

where ρ is the density, $\boldsymbol{u}$ the velocity, $\boldsymbol{m}$ $(= \rho \boldsymbol{u})$ is the mass flux, $\boldsymbol{\xi} = \boldsymbol{\nabla} \times \boldsymbol{u}$ is the vorticity, $\boldsymbol{\zeta} = \boldsymbol{\xi} \times \boldsymbol{u}$, H is the total enthaply and $\boldsymbol{n}$ is the normalized outward normal to S. For all variables, the classical Reynolds decomposition is used: $\phi = \overline{\phi} + \phi'$. On the right-hand side of equation (1), the Rayleigh term, R, represents the contribution of combustion, while D, accounts for the interaction between acoustics and vortices. They take the form:

DOI: 10.13009/EUCASS2017-609

$$R = \int_V \overline{\left(\frac{\alpha}{\rho c_p}\right)} \left(p'q' + \overline{p'q'}\right) dV \tag{4}$$

$$D = -\int_V \left(\boldsymbol{m}' \cdot \zeta' + \overline{\boldsymbol{m}' \cdot \zeta'}\right) dV, \tag{5}$$

where α is the coefficient of thermal expansion, c_p the constant-pressure specific heat capacity, p the pressure and q the heat release rate.

The sign of R and D is not known a priori. The seminal work of Rayleigh[4] states that $R > 0$ is a necessary condition for a combustion instability to grow. Regarding equation (5), $D > 0$ corresponds to coherent flow structures producing disturbance energy, which is the mechanism driving jet and cavity noise. Conversely, $D < 0$ indicates a damping of disturbance energy by vorticity.

3.1 Temporal evolutions

It is now relevant to study the temporal evolutions of E_d, R and D in order to discuss the stability of LP1 and LP4. As explained by Urbano et al.[18] the two operating conditions were submitted to increasing levels of initial pressure perturbation, mimicking a so-called bomb test used for the certification of engines. Figure 3(a) presents the evolution

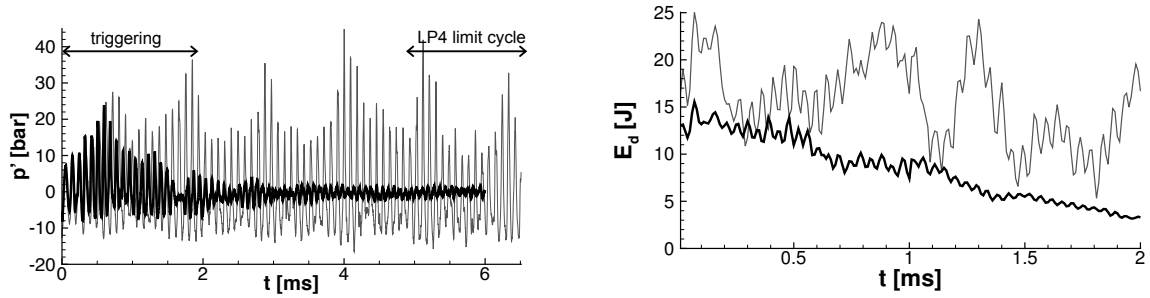

(a) Pressure fluctuations.

(b) Disturbance energy.

Figure 3: Temporal evolution of pressure fluctuations and disturbance energy for LP1 (——) and LP4 (——) in the LES.

of pressure fluctuations p', for the two cases. It is found that LP1 returns to a stable operating condition in around 3 ms while LP4 locks on a large-amplitude limit cycle. The corresponding evolution of disturbance energy (only for the first 2 ms) is given in Fig. 3(b). It appears that LP1 shows a continuous decrease of E_d, while large values are sustained for LP4, despite some low-frequency fluctuations that are not discussed here.

The two source term on the r.h.s of equation 1 are now studied. The Rayleigh term plotted in Fig. 4(a) shows that for both operating conditions, unsteady combustion is feeding disturbance energy. This means that from the classical Rayleigh index analysis, both LP1 and LP4 are potentially unstable. Shortly after the triggering, say around $t = 0.5$ ms, R is comparable for both cases. The subsequent decay for LP1 is caused by the lower levels of acoustic fluctuations. The evolutions of the D term shown in Fig. 4(b) are fairly different for the two cases. For LP1, D is consistently positive, indicating that the coupling between acoustics and vorticity is a source of noise. It is important to note that for LP1, both D and R are positive so that it is only thanks to the fluxes, F, through the boundaries that this operating point is stable. Regarding LP4, both positive and large negative values of D are reached (with a slightly negative mean) indicating that this term is on average close to neutral.

3.2 Maps of acoustic energy source terms

The temporal evolution of the spatially-averaged contributions of R and D is now complemented by a spatial and spectral analysis. For this purpose, the combustion chamber is divided in 42 sub-volumes, each enclosing a single flame. The boundary of these are at equal distance from neighbouring injectors and contain the whole length of the combustion chamber. Equations 4 and 5 are used to determine the contribution of individual flames to R and D at the frequency of each of the two dominant modes. For this analysis, we use the procedure of Urbano et al.,[27] which neglects non-linear interactions between modes. The results are presented in Fig. 5 for the Rayleigh term in the form of

DOI: 10.13009/EUCASS2017-609

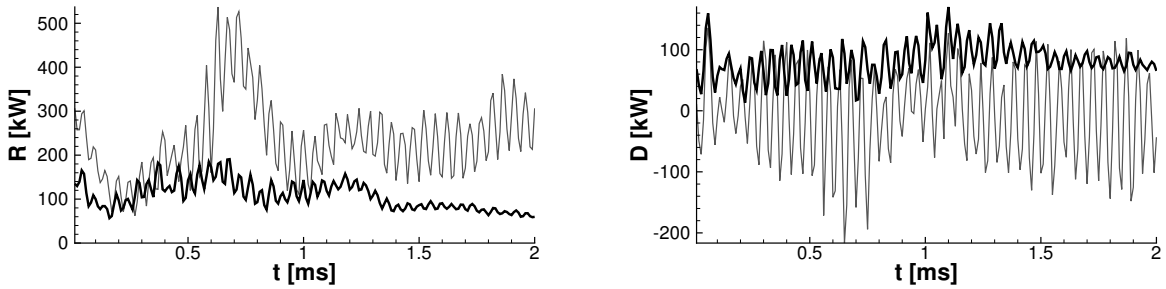

(a) Rayleigh term. (b) Vorticity coupling term.

Figure 4: Temporal evolution of Rayleigh and vorticity coupling terms for LP1 (——) and LP4 (——) in the LES.

transverse cuts through the chamber where the injectors and the boundaries between the sub-volumes are drawn. Each volume is then coloured according to the intensity of R. Figure 5(a) corresponds to the magnitude of R at the frequency

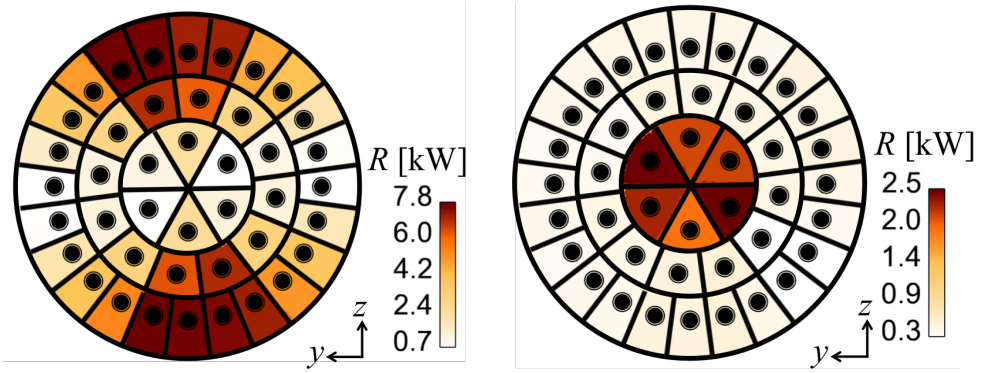

(a) Transverse mode. (b) Radial mode.

Figure 5: Maps of Rayleigh term for the two dominant modes during the limit cycle of LP4.

of the 1T mode. All injectors have a positive contribution, which is consistent with the temporal evolution of Fig. 4(a). A qualitative comparison with Fig. 2(a) indicates that the flames located near the pressure anti-node respond with the most intensity, while those close to the pressure nodal line have the smallest R. The contribution of R at the frequency of the 1R mode is plotted in Fig. 5(b). Again, the flames located on the nodal line (second ring of injectors) respond weakly whereas those near the central pressure antinode have the largest magnitude. However, the outer flames, which are also at a pressure antinode have a low response. This may be caused by a different delay of these flames versus the ones at the center.

The global picture emerging from the analysis of Fig. 5 is that regarding the coupling between combustion and disturbance energy, these coaxial diffusion flames respond weakly to transverse velocity fluctuations and strongly to bulk pressure variations.

We now turn to the analysis of the D term, which is plotted in Fig. 6. Unlike the Rayleigh term, the coupling between acoustics and vorticity produces both positive and negative contributions. For the 1T mode (Fig. 6(a)) the negative contribution clearly dominates and is located in a vast region around the pressure nodal line. This means that in these regions, disturbance energy is damped by the D term. Nevertheless, D is positive near the pressure antinodes. The configuration is similar for the 1R mode Fig. 6(b)) where, again, negative values of D are found near the nodal line.

In summary, the spatial and spectral analysis of the flame contributions to the evolution of the disturbance energy draws a precise picture of the driving and damping mechanisms involved in the overall growth of a combustion instability. The sustained level of disturbance energy is the result of a complex balance between the two source terms describing the interaction of acoustic waves with combustion (R) and vortices (D). Flames located near the pressure nodal line show large levels of negative D and small levels of positive R so that their contribution is stabilising. Conversely, flames located near the pressure antinodes, where pressure fluctuation levels are highest, exhibit large values

DOI: 10.13009/EUCASS2017-609

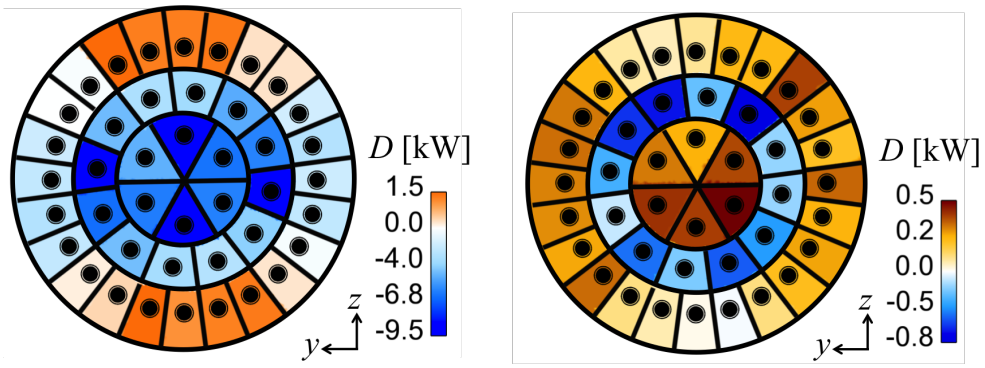

(a) Transverse mode. (b) Radial mode.

Figure 6: Maps of vorticity coupling term for the two dominant modes during the limit cycle of LP4.

of R and relatively small but positive values of D so that their net contribution is destabilising.

4. Single flame computations

The analysis conducted in Sec. 3 indicates that the coaxial diffusion flames typically used in liquid rocket engines respond in a fairly complex way to transverse acoustic modes. The overall picture is that the flames driving the instability are those near the pressure antinode, which in fact only experience a bulk pressure fluctuation at the injector outlet and negligible transverse velocity fluctuations. It was speculated by Urbano et al.[18] that these flames do not directly respond to the pressure fluctuation but rather to the subsequent fluctuations of reactants' mass flow rates. As a consequence, it is assumed that the study of a single flame submitted to fluctuating flow rate could be relevant for the understanding of the physical mechanisms driving the response of flames located at a pressure antinode in a transverse mode. In this Section, we present preliminary results in this line of thought.

The computational domain and mesh are presented in Fig. 7. The fuel and oxidiser manifolds have been cut out and only a short length of the injector was kept. The length of the combustion chamber is equal to that of the full engine (cf. Fig. 7(a)) and in order to maintain the confinement of the flame, the cross-section corresponds to 1/42 of the real chamber. A zoom on the mesh in the near-injector region is shown in Figs. 7(b) and 7(c). The resolution in the wake

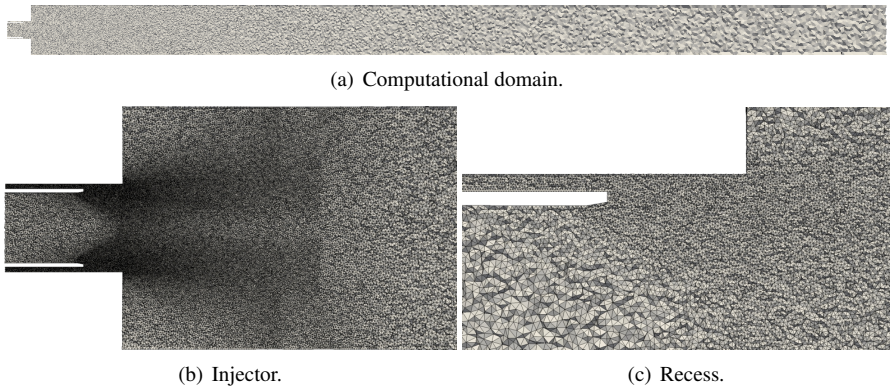

(a) Computational domain.

(b) Injector. (c) Recess.

Figure 7: Longitudinal cuts through the mesh for the LES of the single injector.

of the lip separating the two streams is $\Delta = 35\ \mu$m and it is kept over one injector diameter. The mesh is then slowly coarsened. Finally, this computation is performed with the exact same numerical parameters and models as that of the full engine and only the operating conditions of LP4 are considered.

The dynamics of this type of flame is very strong, even under steady-state conditions. Indeed, the large velocity difference between the hydrogen ($u_{H_2} = 318$ ms^{-1}) and oxygen ($u_{O_2} = 12.9$ ms^{-1}) streams generates a strong shear enhancing the heat release rate and favouring the development of vortices. An instantaneous iso-surface of the temperature field is shown in Fig. 8. In the recessed region, the flame remains almost cylindrical but at the entrance of the

DOI: 10.13009/EUCASS2017-609

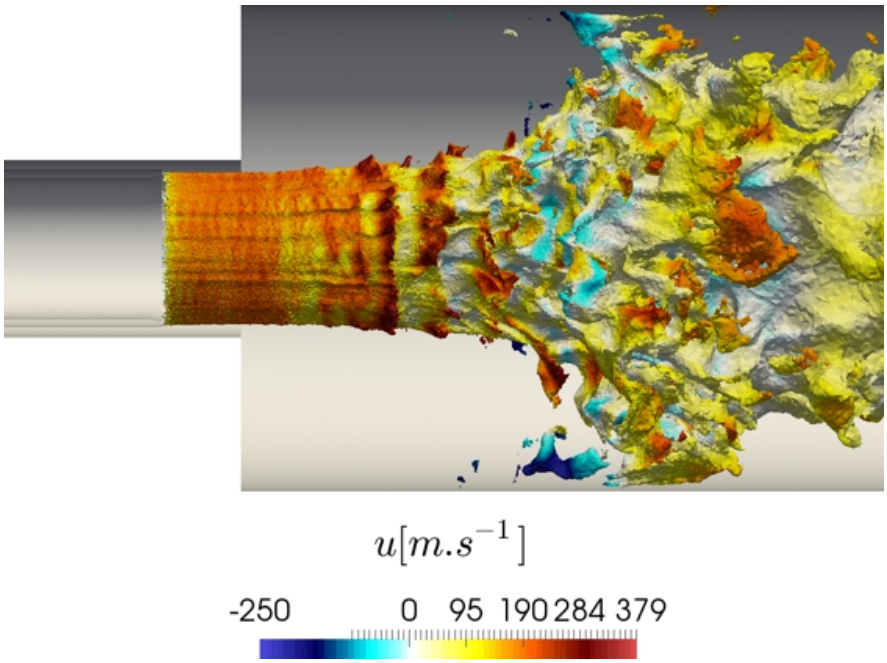

Figure 8: Instantaneous temperature iso-surface coloured by axial velocity, without acoustic forcing.

combustion chamber, vortical structures quickly develop. After two injector diameters, the flame expands abruptly, a behaviour typically observed in experiments under these conditions. Downstream of this sudden expansion, the flame is much less convoluted as seen at the far right of Fig. 8.

Once the flame length is statistically converged (in this case after 25 ms, which corresponds to 1.5 flow-through time of the oxygen stream), the configuration is submitted to acoustic fluctuations. As shown in Sec. 3.2, the flames responding the most to the transverse mode are those located at a pressure anti-node. Consequently, forcing a single flame with a bulk pressure fluctuation may be a valid procedure. However, it is suspected that the actual mechanism through which the flame responds involves velocity fluctuations in the oxygen and/or hydrogen streams. In this preliminary study, we focus on the influence of hydrogen velocity fluctuations. Indeed, because the hydrogen stream is much faster, at similar levels of relative fluctuations, the variations of shear stress and strain on the flame can be expected to be larger. These parameters are known to favour the formation of vortical structures and increase the reaction rates, two mechanisms usually involved in the unsteady flame response.

We choose here to force the hydrogen stream at 15 % of its bulk velocity, which is in the range observed in the LES of the full engine.[28] The frequency is that of the first transverse mode, which is unstable for LP4. Figure 9 compares instantaneous fields of the forced and unforced cases. An iso-surface of density (ρ = 500 kg.m^{-3}) illustrates the dynamics of the dense oxygen jet and a longitudinal cut of instantaneous temperature shows the shape of the flame. The differences in the temperature fields are not obvious on these snapshots: both show a fairly flat flame in the recessed region, followed by an intense wrinkling at the region of sudden expansion. the flame then becomes smoother. However, the dense oxygen cores appear qualitatively different. For the case without acoustic forcing (Fig. 9(a)), small-scale wrinkles are formed from the beginning of the mixing layer. Theses structures grow and merge to form structures of the same size as the jet diameter around the location of the flame radial expansion. For the forced case (Fig. 9(b)), the small-scale structures are not apparent in the early stages. Instead, structures of roughly constant wavelength grow after the recessed region, which are dictated by the frequency of the acoustic forcing. The dense core length appears to be shortened which must be confirmed on averaged fields. At this point is the study, only a qualitative analysis has been performed. In the next steps, time series of heat release rate will be used to measure the gain and phase of the flame response.

5. Conclusion

In this paper, Large-Eddy Simulations of coaxial hydrogen/oxygen flames under supercritical thermodynamic conditions have been analysed. The objective was to understand the mechanisms driving the flame response under a transverse combustion instability in a liquid-propellant rocket engine. In a first part, a preexisting LES of a 42-injector

DOI: 10.13009/EUCASS2017-609

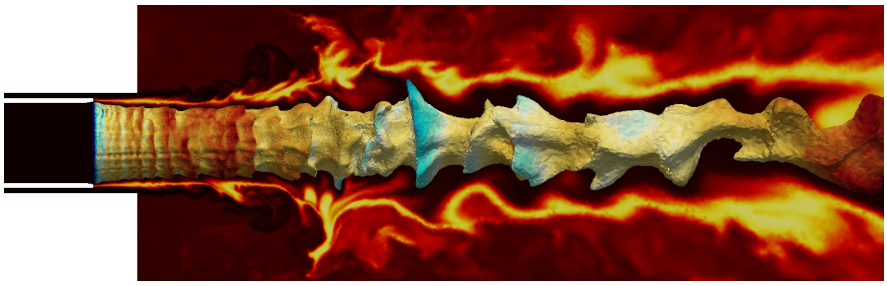

(a) No acoustic forcing.

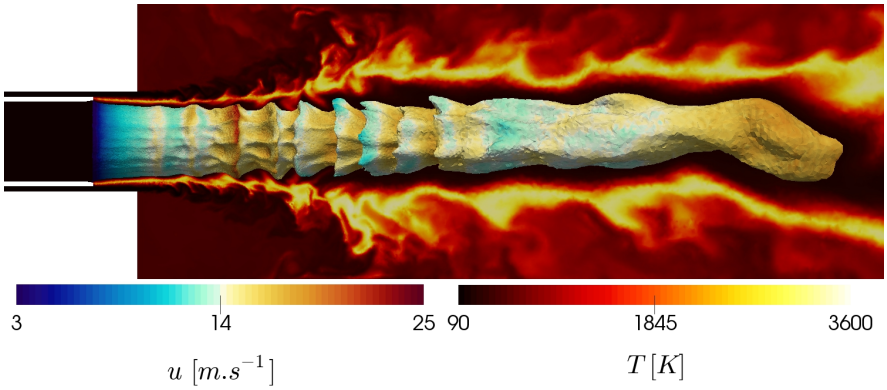

(b) Acoustic forcing of hydrogen stream.

Figure 9: LES of the single injector: longitudinal cut of temperature and iso-surface of density (ρ = 500 kg.m^{-3}) coloured by axial velocity.

engine was analysed in the framework of disturbance energy. A stable and an unstable operating condition were considered showing that despite a positive Rayleigh index in both cases, the different stability is caused by the interaction between acoustics and vorticity. Then maps of these two terms showed that the flames responding the most to the transverse acoustic mode are located at a pressure antinode. The flames near the pressure nodal line, submitted to transverse velocity fluctuations have a smaller contribution to the total Rayleigh index. Moreover, it was shown that the flapping motion of the flames induced by the transverse velocity provides large dissipation of the disturbance energy corresponding to a stabilisation effect on the combustion instability. Finally, a preliminary study of a single-injector configuration illustrated how the flame responds to a pulsation in the hydrogen stream with the formation of large coherent structures at the edges of the dense oxygen core. Further studies will be dedicated to the quantification of the flame response, through Flame Transfer Functions, as well as the comparison of the response to hydrogen and oxygen stream pulsation.

6. Acknowledgments

This work was granted access to the high-performance computing resources of CINES under the allocation 2017-A0012B07036 made by Grand Equipement National de Calcul Intensif.
The research leading to these results has received funding from the European Research Council under the European Union's Seventh Framework Programme (FP/2007-2013) / ERC Grant Agreement ERC-AdG 319067-INTECOCIS.

References

[1] Fred E. C. Culick. Combustion instabilities in liquid-fuelled propulsion systems. In *AGARD 72B PEP Meet.*, number 450, pages 1–74, 1988.

[2] William E. Anderson and Vigor Yang. *Liquid Rocket Engine Combustion Instability*. Number 169. American Institute of Aeronautics and Astronautics, Washington DC, progress i edition, jan 1995.

DOI: 10.13009/EUCASS2017-609

[3] Joseph C Oefelein and Vigor Yang. Comprehensive Review of Liquid-Propellant Combustion Instabilities in F-1 Engines. *J. Propuls. Power*, 9(5):657–677, 1993.

[4] John William Strutt Rayleigh. The explanation or certain acoustic phenomena. *Nature*, 18:319, 1878.

[5] Tim C Lieuwen. *Unsteady Combustor Physics*. Cambridge University Press, 2012.

[6] Thierry Poinsot and Denis Veynante. *Theoretical And Numerical Combustion*. www.cerfacs.fr/elearning, third edition, 2011.

[7] David T. Harrje and Frederick H. Reardon. Liquid Propellant Rocket Combustion Instability. Technical report, 1972.

[8] Geoffrey Searby, Aurélie Nicole, Mohammed Habiballah, and Emmanuel Laroche. Prediction of the Efficiency of Acoustic Damping Cavities. *J. Propuls. Power*, 24(3):516–523, may 2008.

[9] D You, David D Ku, and V Yang. Acoustic Waves in Baffled Combustion Chamber with Radial and Circumferential Blades. *J. Propuls. Power*, 29(6):1–15, 2013.

[10] Luigi Crocco, David T. Harrje, and Frederick H. Reardon. Transverse Combustion Instability in Liquid Propellant Rocket Motors. *ARS J.*, 32(3):366–373, jan 1962.

[11] William A Sirignano and Pavel P Popov. Two-Dimensional Model for Liquid-Rocket Transverse Combustion Instability. *AIAA J.*, 51(12):2919–2934, aug 2013.

[12] Pavel P. Popov, Athanasios Sideris, and William a. Sirignano. Stochastic modelling of transverse wave instability in a liquid-propellant rocket engine. *J. Fluid Mech.*, 745:62–91, 2014.

[13] E Lubarsky, M Hadjipanayis, D Shcherbik, O Bibik, and BT Zinn. Control of Tangential Instability by Asymmetric Baffle. In *46th AIAA Aerosp. Sci. Meet. Exhib.*, Reno, Nevada, 2008.

[14] Yoann Méry, Layal Hakim, Philippe Scouflaire, Lucien Vingert, Sébastien Ducruix, and Sébastien Candel. Experimental investigation of cryogenic flame dynamics under transverse acoustic modulations. *Comptes Rendus Mécanique*, 341(1-2):100–109, jan 2013.

[15] Justin S. Hardi, Scott K. Beinke, Michael Oschwald, and Bassam B. Dally. Coupling of Cryogenic Oxygen-Hydrogen Flames to Longitudinal and Transverse Acoustic Instabilities. *J. Propuls. Power*, 30(4):991–1004, 2014.

[16] Thomas Sattelmayer, Martin Schmid, and Moritz Schulze. Interaction of Combustion with Transverse Velocity Fluctuations in Liquid Rocket Engines. *J. Propuls. Power*, 31(4):1137–1147, 2015.

[17] L. Hakim, A. Ruiz, T. Schmitt, M. Boileau, G. Staffelbach, S. Ducruix, B. Cuenot, and S. Candel. Large eddy simulations of multiple transcritical coaxial flames submitted to a high-frequency transverse acoustic modulation. *Proc. Combust. Inst.*, 35(2):1461–1468, 2015.

[18] A Urbano, L Selle, G Staffelbach, B Cuenot, T Schmitt, S Ducruix, and S Candel. Exploration of combustion instability triggering using Large Eddy Simulation of a multiple injector Liquid Rocket Engine. *Combust. Flame*, 169:129–140, 2016.

[19] Olivier Colin and Michael Rudgyard. Development of High-Order Taylor-Galerkin Schemes for LES. *J. Comput. Phys.*, 162(2):338–371, aug 2000.

[20] F. Nicoud and F. Ducros. Subgrid-scale stress modelling based on the square of the velocity gradient tensor. *Flow, Turbul. Combust.*, 62(3):183–200, 1999.

[21] Giorgio Soave. Equilibrium constants from a modified Redlich-Kwong equation of state. *Chem. Eng. Sci.*, 27(6):1197–1203, jun 1972.

[22] Ting Horng Chung, Mohammad Ajlan, Lloyd L Lee, and Kenneth E Starling. Generalized multiparameter correlation for nonpolar and polar fluid transport properties. *Ind. Eng. Chem. Res.*, 27(4):671–679, 1988.

[23] T. Schmitt, Y. Méry, M. Boileau, and S. Candel. Large-Eddy Simulation of oxygen/methane flames under transcritical conditions. *Proc. Combust. Inst.*, 33(1):1383–1390, 2011.

DOI: 10.13009/EUCASS2017-609

[24] S. Gröning, D. Suslov, M. Oschwald, and T. Sattelmayer. Stability behaviour of a cylindrical rocket engine combustion chamber operated with liquid hydrogen and liquid oxygen. In *5th Eur. Conf. Aeronaut. Sp. Sci.*, Munich, 2013.

[25] M K Myers. Transport of energy by disturbances in arbitrary steady flows. *J. Fluid Mech.*, 226:383–400, apr 1991.

[26] Michael J. Brear, Frank Nicoud, Mohsen Talei, Alexis Giauque, and Evatt R. Hawkes. Disturbance energy transport and sound production in gaseous combustion. *J. Fluid Mech.*, 707:53–73, jul 2012.

[27] A. Urbano and L. Selle. Driving and damping mechanisms for transverse combustion instabilities in liquid rocket engines. *J. Fluid Mech.*, 820:R2, jun 2017.

[28] A Urbano, Q Douasbin, L Selle, G Staffelbach, B Cuenot, T Schmitt, S Ducruix, and S Candel. Study of flame response to transverse acoustic modes from the LES of a 42-injector rocket engine. *Proc. Combust. Inst.*, 36:2633–2639, jul 2017.